PARAMETRIC STUDY OF A PHASE CHANGE THERMAL STORAGE MODULE

Antonio Ramos Archibold[a,b], Sarada Kuravi[a,c], Muhammad M Rahman[a,b], D. Yogi Goswami[a,c,*],

Elias K. Stefanakos[a,d], José Gonzalez-Aguilar[e], Manuel Romero[e],

[a]*Clean Energy Research Center, University of South Florida, Tampa Florida, USA*
[b]*Department of Mechanical Engineering, University of South Florida, Tampa Florida, USA.*
[c]*Department of Chemical & Biomedical Engineering, University of South Florida, Tampa Florida, USA*
[d]*Department of Electrical Engineering, University of South Florida, Tampa Florida, USA*
[e]*Institute IMDEA Energy, Mostoles, Spain*

Abstract

Concentrated solar power generation has the potential to partially meet the future energy demand and reduce our dependence of fossil fuels. However due to the intermittent nature of this energy source, it has not been used for baseload power. This problem can be solved by implementing an efficient, economical and reliable latent heat (LH) energy storage strategy. An accurate heat transfer analysis will play an important role to make this strategy successful. This work presents a 2D numerical model of the diffusion-natural convective controlled heat transfer during an unconstrained (solid–liquid density difference) melting process of an encapsulated spherical thermal energy storage (TES) capsule filled with an inorganic salt as the phase change material (PCM). The melting of the PCM was modeled using the finite volume numerical procedure with a single-domain enthalpy formulation. Transient numerical simulations were performed using the CFD software Ansys-Fluent V 12.1. A detailed parametric analysis was carried out in order to analyze the geometrical and operational effects of the system and their influence on the charging times. The study focused on PCMs with melting point between 300°C to 400°C and metal coating materials subjected to a uniform wall temperature from 73°C to 93°C above the mean melting temperature of the PCM. The temperature profiles and interface positions for different Rayleigh, Stefan and Fourier numbers are determined. Computational results of this study show that for a fixed Stefan number (Ste=0.694) there is a significant difference in the flow fields for cases with Rayleigh number from $9.17x10^6$ to $7.33x10^7$.

Keywords: Energy storage, Latent heat, Renewable energy, Heat transfer.

1. INTRODUCTION.

The use of latent heat storage devices (LHSD) is one of the most promising technique that can play a preponderant role in solar power technologies as a strategy to enhance the effective energy management, i.e. effective thermal energy utilization under the seasonal and intermittent nature of solar energy. This advantage could be achieved since it became of a considerably higher energy storage density compared to sensible heat storage systems and has the capacity to capture and release energy as latent heat of fusion at a constant temperature or over a limited temperature range corresponding to the melting point of the phase change material. According to Dutil et al.(2010) and Medrano et al. (2010) such devices and systems also improve the performance and reliability of the plant by satisfying peak loads and allowing systems to work within an optimal and stable range. Based on that, an accurate heat transfer analysis for the melting and solidification process within the phase change material is required in order to develop an optimal design and predict operational conditions of the LHSD. The aim of the present study is to develop a numerical model of the heat transfer during the melting process of a spherical capsule filled with sodium nitrate considering conduction, natural convection and solid–liquid density difference.

A considerable amount of experimental, theoretical and numerical studies have been reported in the literature on the heat transfer phenomena of melting and freezing process of PCM's that are stored within containers of different shapes. Grimado and Boley (1970) presented a numerical procedure of the diffusion-controlled heat transfer during the melting process of a sphere. The outer surface was subjected to a spherically symmetric and time dependent heat flux boundary condition. Melting rate and temperature distribution for different metals was estimated. Nicholas and Bayazitoğlu (1980)

*Address all correspondence to this author

A_{mu} porosity constant $[kg/m^3 s]$
c_p specific heat at constant pressure $[J/kg\ K]$
Da Darcy number, defined as $\mu\lambda^3/CR^2(1-\lambda)^2$
Fo Fourier number defined as $[\alpha t/R^2]$
g gravitational aceleration $[m/s^2]$
H sensible enthalpy $[kJ/kg]$
ΔH latent heat $[J/kg]$
k thermal conductivity $[W/m\ K]$
L latent heat of fusion $[J/kg]$
Pr Prandtl number of the fluid, defined as $[\nu/\alpha]$
R_i inner radius of the container $[m]$
R_o outer radius of the container $[m]$
Ra Rayleigh number defined as $8g\beta(T_w - T_m)R^3/\nu\alpha$
S source term in momentum equation
Ste Stefan number defined as $c_p(T_w - T_m)/L$
t time $[sec]$
T temperature $[K]$
T_i initial temperature of the PCM $[K]$
T_m melting temperature of the PCM $[K]$
T_w surface temperature of the enclosure $[K]$
ϑ_i velocity component $[m/s]$

Greek Symbols

α Thermal diffusivity $[m^2/s]$
β Thermal expansion coefficient $[K^{-1}]$
λ Liquid/solid fraction
ρ Density $[kg/m^3]$
μ Dynamic viscosity $[kg/m\ s]$
ν kinenamic viscosity $[m^2/s]$

Subscripts

l liquidus
m melting
r radial direction
s solidus
w wall

presented a numerical analysis of the effect of unequal densities on the shape and location of the solid-liquid interface during heat diffusion-controlled melting process for a system within a horizontal cylindrical isothermal enclosure. The finite difference method was used to find the dimensionless transient temperature profile in the liquid medium and the position and rate of movement of the solid-liquid interface. However the analysis neglected the convective heat transfer during the phase change process. Later on Moore and Bayazitoglu (1982) investigated the unconstrained diffusion-natural convection controlled melting process of n-octadecane wax within a spherical enclosure. The energy and interface equations were solved using the finite difference technique. Good agreement was found between the numerical results and the experimental data for $Ste = 0.05$ and 0.1 with a maximum deviation of about 10 percent in the predicted interface position. Based on the energy stored results the study also concluded that the convective effects can be neglected only at small Stefan numbers below than 0.1.

Bahrami and Wang (1987) presented an approximate closed-form solution of conduction-driven melting within spheres by the use of assumptions similar to the theories of lubrication and film condensation. The effects of gravitational force resulting from unequal solid and liquid densities and the decoupled temperature and velocity fields were considered. The agreement between the theory and the experiments appears to be reasonable for small values of $Fo \cdot Ste$. The agreement decreased for larger $Fo \cdot Ste$ values with the experimental data laying approximately 20 percent below the theory. Melting process in spherical containers has been studied further by Roy and Sengupta (1987) who reported an analytical solution for the melting rate at the lower surface of the solid core based on the technique originally developed for the cylindrical geometry by Bareiss and Beer(1984). Heat transport was controlled by heat conduction only. The predicted melting rate showed good agreement with the experimental data published by Moore and Bayazitoglu (1982) with maximum deviation of 16 percent for $Ste = 0.05$ and 0.1. Later on Roy and Sengupta (1990) analytically studied the effect of natural convection within the thin melting layer in the bottom of the sphere and within the top part of the solid core during the unconstrained melting process with an isothermal boundary. The analysis concluded that a significant amount (15% for typical cases) of melting takes place at the upper surface of the solid core. Also the effects of Grashof and Prandtl numbers in the upper region are smaller than the values commonly encountered in natural convection on spherical geometries.

Saitoh and Kato (1993) reported experimental and numerical results on the melting in horizontal cylindrical capsules with both close-contact and natural convective heat transfer. The experimental setup consisted of copper cylindrical tubes with diameters of 0.04, 0.1 and 0.2 m filled with $n-octadecane$ as the PCM material mounted in a constant temperature bath. Based on the melting front results indicated that with the increase of the Stefan number the contribution of natural convection becomes more significant. Fomin and Saitoh (1999) presented a numerical and analytical investigation of the close-contact melting within a spherical capsule with a non-isothermal wall. The analytical solution method used in their investigation is an extension of the mathematical approach developed by Bareiss and Beer (1984) and the numerical model was solved by utilizing the boundary fixing method. The wall temperature boundary condition was specified by a sinusoidal function. They found that the increase of the temperature distribution leads to a higher melting speed for

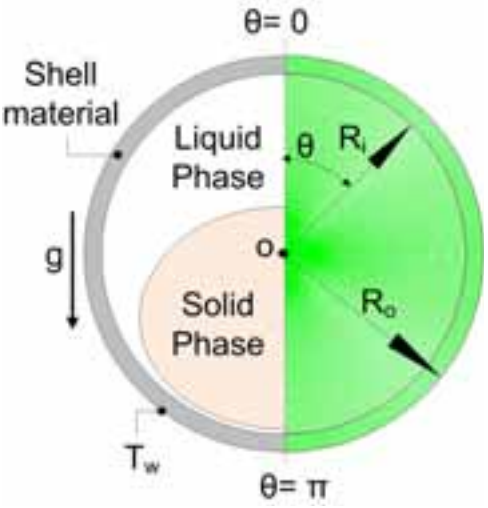

Figure 1: Schematic diagram of the physical model.

$Ste = 0.5$. Khodadadi and Zhang (2001) performed a computational study of the combined conduction and buoyancy-driven convection on constrained melting of PCM's within spherical containers with an isothermal boundary. The study focused on low-Prandtl number fluids and used silicon as a PCM. The results were obtained through simulations based on the finite-volume procedure and the phase change phenomenon was modeled by single-domain enthalpy formulation. Three cases ($case\ a,\ Ra = 1.428x10^5, case\ b,\ Ra = 1.143x10^6\ and\ case\ c,\ Ra = 1.151x10^7$) were analyzed in order to assess the role of the Rayleigh number on the melting process. The total melting time was 8% shorter for Case (a), 15% shorter for Case (b), and 40% shorter for Case (c) when compared to the corresponding diffusion-controlled melting processes. Also the study analyzed the effect of Stefan number during the melting process. It was concluded that the flow and thermal fields are very similar for cases with Stefan number from 0.0267 to 0.0533 and fixed Raleigh and Prandtl numbers. Also as buoyancy-driven convection became more dominant due to the growth of the melt zone, accelerated melting in the top region of the sphere in comparison to the bottom zone was observed.

Assis et al. (2007) reported a numerical and experimental study of the melting process in spherical enclosures of 40, 60 and 80mm in diameter subjected to constant wall temperatures. The numerical model takes into account the volume expansion due to melting, the density change between the phases and the convective heat transfer in the fluid media. RT27 (Rubitherm GmbH) was used as the PCM. In order to model the volumetric expansion a PCM-air computational domain was defined. Initially solid PCM fills 85% of the enclosed space while the remaining 15% is filled by air. The enthalpy-porosity approach was used to model the melting process. The melt fraction was presented as a function of a combination of the Fourier, Stefan and Grashof numbers, namely, $FoSte^{1/3}Gr^{1/4}$. The investigation concluded that all the study cases, except that for $Ste = 0.2$, practically merge into a single curve. Tan et al. (2009) discussed a combined experimental/computational study of the effect of buoyancy-driven convection on the melting process in spherical containers. Density differences of the liquid and solid phases were neglected in the mathematical simulations. Paraffin wax $n-octadecane$ was used as the PCM. The single domain enthalpy-porosity formulation was used to model the melting process. In the study, computational findings were verified through qualitative observations of the phase change pattern during constrained melting of the PCM. It was shown that even though the computational technique captures the trends of the constrained melting of the sphere, it predicts a faster rate of melting. Also computational results reveal a waviness and excessive melting of the bottom part of the PCM.

In this study, a parametric analysis of the 2D melting in a spherical cavity was carried out in order to investigate the effect of the Rayleigh and Stefan numbers on the melting rate of the PCM. Special emphasis is placed on the fact that, to the best of the authors knowledge, the melting process of spherical encapsulated sodium nitrate has been rarely investigated in the literature.

2. Physical and mathematical model.

A spherical shell of inner and outer radii R_i and R_o, respectively, is initially filled with a solid PCM at a temperature T_i. For time $t > 0$, the outer surface of the shell is exposed to a constant temperature T_w, which is greater than the melting temperature of the PCM. Heat is transferred by conduction through the wall of the capsule and melting process initiates at the inner surface with the solid-liquid interface moving into the PCM. A schematic representation of the considered physical model is shown in the left hand side of Figure 1.

Table 1: Governing equations.

Equation		
Continuity	$\frac{\partial \rho}{\partial t}+\frac{1}{r^2}\frac{\partial}{\partial r}(\rho r^2 \vartheta_r)+\frac{1}{rsin\theta}\frac{\partial}{\partial \theta}(\rho \vartheta_\theta sin\theta)=0$	(1)
Radial direction momentum	$\frac{\partial \vartheta_r}{\partial t}+\frac{1}{r^2}\frac{\partial}{\partial r}(\vartheta_r r^2 \vartheta_r)+\frac{1}{rsin\theta}\frac{\partial}{\partial \theta}(\vartheta_\theta sin\theta \vartheta_r)=\nu\left(\frac{1}{r^2}\frac{\partial}{\partial r}\left(r^2\frac{\partial \vartheta_r}{\partial r}\right)+\frac{1}{r^2 sin\theta}\frac{\partial}{\partial \theta}\left(sin\theta\frac{\partial \vartheta_r}{\partial \theta}\right)\right)-\frac{1}{\rho}\frac{\partial P}{\partial r}+g\beta(T-T_m)cos\theta+\frac{\vartheta_\theta^2}{r}-\frac{2\nu}{r^2}\frac{\partial \vartheta_\theta}{\partial \theta}-\frac{2\nu cot\theta}{r^2}\vartheta_\theta-\frac{2\nu}{r^2}\vartheta_r-\frac{A_{mu}(1-\lambda)^2}{\rho(\lambda^3-\varepsilon)}\vartheta_r$	(2)
Polar direction momentum	$\frac{\partial \vartheta_\theta}{\partial t}+\frac{1}{r^2}\frac{\partial}{\partial r}(\vartheta_r r^2 \vartheta_\theta)+\frac{1}{rsin\theta}\frac{\partial}{\partial \theta}(\vartheta_\theta sin\theta \vartheta_\theta)=\nu\left(\frac{1}{r^2}\frac{\partial}{\partial r}\left(r^2\frac{\partial \vartheta_\theta}{\partial r}\right)+\frac{1}{r^2 sin\theta}\frac{\partial}{\partial \theta}\left(sin\theta\frac{\partial \vartheta_\theta}{\partial \theta}\right)\right)-\frac{1}{\rho}\frac{1}{r}\frac{\partial P}{\partial \theta}-g\beta(T-T_m)sin\theta-\frac{\vartheta_r\vartheta_\theta}{r}+\nu\frac{2}{r^2}\frac{\partial \vartheta_r}{\partial \theta}-\frac{\nu}{r^2 sin^2\theta}\vartheta_\theta-\frac{A_{mu}(1-\lambda)^2}{\rho(\lambda^3-\varepsilon)}\vartheta_\theta$	(3)
Energy	$\frac{\partial h}{\partial t}+\frac{1}{r^2}\frac{\partial}{\partial r}(\vartheta_r r^2 h)+\frac{1}{rsin\theta}\frac{\partial}{\partial \theta}(\vartheta_\theta sin\theta h)=\frac{k}{\rho c_p}\left(\frac{1}{r^2}\frac{\partial}{\partial r}\left(r^2\frac{\partial h}{\partial r}\right)+\frac{1}{r^2 sin\theta}\frac{\partial}{\partial \theta}\left(sin\theta\frac{\partial h}{\partial \theta}\right)\right)-\frac{1}{\rho c_p}\left(\frac{\partial h}{\partial t}+\frac{1}{r^2}\frac{\partial}{\partial r}(\vartheta_r r^2\triangle H)+\frac{1}{rsin\theta}\frac{\partial}{\partial \theta}(\vartheta_\theta sin\theta\triangle H)\right)$	(4)

The following assumptions are made for the mathematical model: (1) both the solid and liquid phases are homogeneous and isotropic, (2) the flow in the capsule is axisymmetric around the vertical axis of the sphere and two dimensional spherical polar coordinate system (r, θ)can be employed, (3) the liquid phase was assumed as a Newtonian fluid with laminar flow, (4) the Boussinesq approximation is used to analyze the buoyancy induced motion in the melt, (5) the viscosity and thermal conductivity of molten sodium nitrate were defined as functions of temperature. Thermophysical properties and process parameters are listed in Table 2.

2.1 Mathematical formulation

Given the above assumptions, the continuity, momentum and energy equations in the spherical coordinates (r and θ radial and polar direction respectively) are presented in Table 1.
A significant effort was directed into the methods used to track the continuously moving boundary of the solid liquid interface and the associated thermophysical property change over the discrete grid of nodes that define the numerical method. According to Voller et al. (2006), the existing modeling methods for such problems can be divided into three groups: fixed grid schemes, deforming grid schemes and hybrid methods. In this study the enthalpy formulation (Eyres et al. (1946) and Price and Slack (1954)), that is one of the fixed grid class methods was employed. The enthalpy function is defined as the sum of the sensible heat h and the latent heat ΔH required for a phase change as follows.

$$H = h + \Delta H \tag{5}$$

where

$$h = h_{ref} + \int_{T_{ref}}^{T} c_p dT \tag{6}$$

Where h_{ref} and T_{ref} are the reference sensible heat and temperature, respectively. As mentioned, the single domain enthalpy-porosity technique, originally introduced by Voller and Prakash (1987) and Brent et al. (1988) was used to track the liquid-solid front inside the PCM. The method considers computational cells in which phase change is occurring as a pseudo porous media, with porosity $\lambda = liquid/solid\ fraction$ decreasing from 1 to 0 as the latent heat content decreases from L to 0. A linear relationship between the latent heat and temperature is used, i.e., $\Delta H = \lambda L$, where L is the latent heat of fusion and the liquid/solid fraction (λ) is used in every cell based on the following relations:

$$\begin{cases} \lambda = 0, & T < T_s \\ \lambda = \dfrac{T - T_s}{T_l - T_s}, & T_s < T < T_l \\ \lambda = 1, & T > T_l \end{cases} \tag{7}$$

The above procedure is accomplished using a Darcy's law-type of porous medium treatment of Voller and Prakash to modify the momentum equation. In this way, on prescribing a "Darcy" source term the velocity value arising from the solution of the momentum equations is inhibited, reaching values close to zero on complete solid formation. The Darcy damping term is the last component in the source term in Eqs (2) and (3) and is defined as:

$$S = A_{mu}\frac{(1-\lambda)^2}{(\lambda^3+\varepsilon)}\vartheta_i \tag{8}$$

where $\varepsilon = 0.001$ is a small computational constant used to avoid division by zero, and A_{mu} is a constant reflecting the morphology of the melt front. This constant is a large number, usually 10^4–10^7. In the present study a value of $C = 10^5\ kg/m^3 s$ has been used.

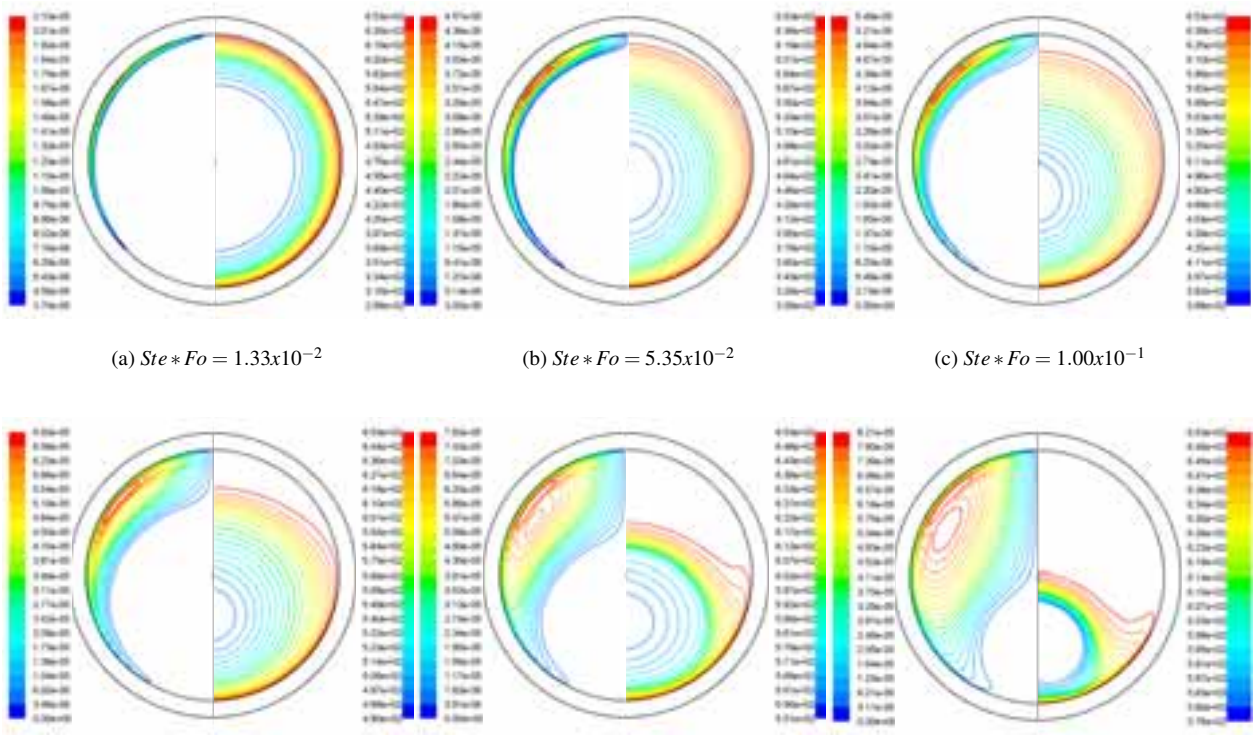

(a) $Ste*Fo = 1.33x10^{-2}$ (b) $Ste*Fo = 5.35x10^{-2}$ (c) $Ste*Fo = 1.00x10^{-1}$

(d) $Ste*Fo = 1.81x10^{-1}$ (e) $Ste*Fo = 2.68x10^{-1}$ (f) $Ste*Fo = 3.48x10^{-1}$

Figure 2: Computed streamlines and temperature contours for case P_2 at different time instants.

Table 2: Thermophysical properties and process parameters.

Parameter	Value	Reference values	Ref.
Sodium nitrate			
Density (kg/m^3)	$\rho = \rho_l/\beta(T-T_l)+1$ $580\ K < T < 673\ K$	$\rho_l = 1950 kg/m^3$ $\beta = 6.6x10^{-4} K^{-1}$ $T_l = 580\ K$	Wang et al.(2010)
Liquid viscosity $(mPa \cdot s)$	$ln\hat{\mu} = 26.689 - \frac{97.54}{\hat{T}} + \frac{112.5}{\hat{T}^2} - \frac{41.70}{\hat{T}^3}$ $580\ K < T < 750\ K$	$\hat{\mu} = \mu(T)/2.98 mPa \cdot s$ $\hat{T} = T/580\ K$	Nunes et al.(2006)
Thermal conductivity $(W/m\ K)$	$k_l = 0.04184(13.5+0.0114(T-579))$ $613\ K < T < 693\ K$ $k_s = 0.04184(13.5+0.008(T-503))$ $300\ K < T < 580\ K$		White and Davis(1967)
Specific heat $c_{p,s} \approx c_{p,l} (J/kg\ K)$	1730		Wang et al.(2010)
Latent heat of fussion (J/kg)	182000		Wang et al.(2010)
$T_s(K)$	577		
$T_l(K)$	298		
Aluminum			
Thermal conductivity $(W/m\ K)$	202.4		Dewitt et al.(1996)
Specific heat $(J/kg\ K)$	871		Dewitt et al.(1996)
Density (kg/m^3)	2719		Dewitt et al.(1996)

3. Computational Procedure

The governing equations were solved using the semi-implicit method for pressure-linked Navier-Stokes equations (SIMPLE) in a segregated fashion based on the commercial software Ansys/Fluent 12.1. The computational domain was discretized using a grid system of 14043 quadrilateral cells. Grid size and time step independence of the unsteady solution based on the liquid/solid interface have been checked by considering cases with different grid densities and time steps values. After a detailed comparison process, the results were found independent. The schematic diagram of the computational grid system is shown on the right half of Figure 1. The time step was set to 0.002sec for all the simulations. The Second Order Upwind scheme was employed for solving the momentum equation and the Power Law differencing scheme was used for the energy equation, and the PRESTO scheme was adopted for the pressure correction equation.

Table 3: Cases investigated for the parametric study.

Case	PCM Diameter (mm)	Shell thickness (mm)	$\triangle T$ $(^{\circ}C)$	Rayleigh number	Stefan number
P_1	15	1	93	$1.22x10^7$	0.884
P_2	15	1	73	$9.17x10^6$	0.694
Q_1	20	1	93	$2.90x10^7$	0.884
Q_2	20	1	73	$2.17x10^7$	0.694
S_2	30	1	73	$7.33x10^7$	0.694

The under-relaxation factors for Pressure, Momentum and Liquid fraction were 0.3, 0.01, and 0.9, respectively. Convergence of the solution was checked for each particular time step. Scaled absolute residuals of $1x10^{-4}$, $1x10^{-6}$ *and* $1x10^{-8}$ were set for continuity, velocity components and energy, respectively as convergence criterion. The number of iterations needed to achieve convergence varied between 150 and 300 per time step.

4. Results and Discussion

Five different configurations were analyzed in the simulation process. All of them are summarized in Table 3. Three different PCM diameters of 15mm, 20mm and 30mm were investigated. Also two temperature differences of $73^{\circ}C$ and $93^{\circ}C$ above the mean melting temperature of the sodium nitrate were explored.

In order to study the influence of the Rayleigh number on the melting process, the predicted instantaneous contours of the streamlines and isotherms for cases P_2 and S_2 are presented in Figures 2 and 3 at different dimensionless times defined as a product of the Stefan and Fourier numbers. The streamline contours are shown on the left half of each circle whereas the temperature contours (in K) are drawn on the right half, with the vertical axis of the sphere separating the two fields. Temperature contours start in a concentric ring patterns at the beginning of the melting process (Figs. 2(a) and 3(a)), due to the step change in the wall temperature. According to Zhang et al. (1999) this suggests that during the early periods, the dominant transport phenomena is due to heat conduction, and natural convection plays a small role. For particular dimensionless times higher than 0.1, the isotherms begin to deviate from the concentric ring patterns (Figs. 2(c) and 3(c)), indicating that natural convection starts to influence the melting process.

A more pronounced effect of the Rayleigh number on the melting process of case S_2 was expected when compared to case P_2. However as Figures 2 and 3 indicate the temperature field is getting oblique angle contours at almost the same dimensionless times. A possible reason for the similar trend is the relative small difference between the Rayleigh numbers of the two cases. Even though there is no apparent difference in the thermal fields for cases P_2 and S_2, special attention should be paid on the order of magnitude of the flow field for all dimensionless times. It is clear that the buoyancy-driven convection effect is higher in case S_2 as compared to case P_2.

The predicted melt fraction as a function of the dimensionless time for different configurations is shown in Figure 4. As expected, faster rate of melting was obtained when the temperature difference is higher (higher Stefan number), for each shell diameter. This behavior is illustrated in Fig. 4a. A significant difference in the melting rate of cases P_1 and P_2 was observed for the dimensionless times higher than $1.5x10^{-1}$. Figure 4b shows the melt fraction of the two different PCM sizes for a fixed Stefan number. Similar trends are observed in the three different curves.

The predicted solid/liquid interface evolution is presented in Figure 5 at different dimensionless times. Results are presented for cases P_2 and S_2 and, it is clear that for $Ste * Fo \geq 2.05x10^{-1}$ the solid unmelted zone is shaped as an oblate spheroid located just below the center of the sphere (Fig.5 (d and h)). It can be inferred that due to the recirculating vortex formed between the top region of the solid phase and the inner wall of the capsule, as clearly observed in Figures 2(e) and 3(e), the melting process is more intensive in the upper part of the solid phase.

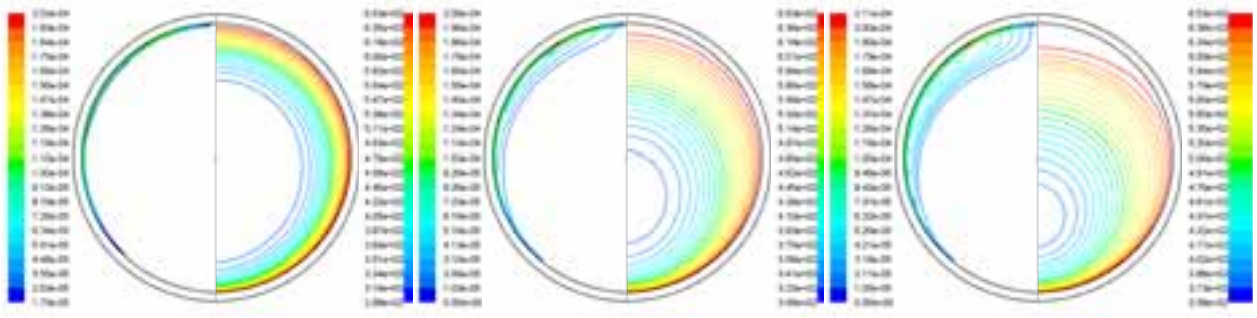

(a) $Ste * Fo = 1.33x10^{-2}$ (b) $Ste * Fo = 5.35x10^{-2}$ (c) $Ste * Fo = 1.00x10^{-1}$

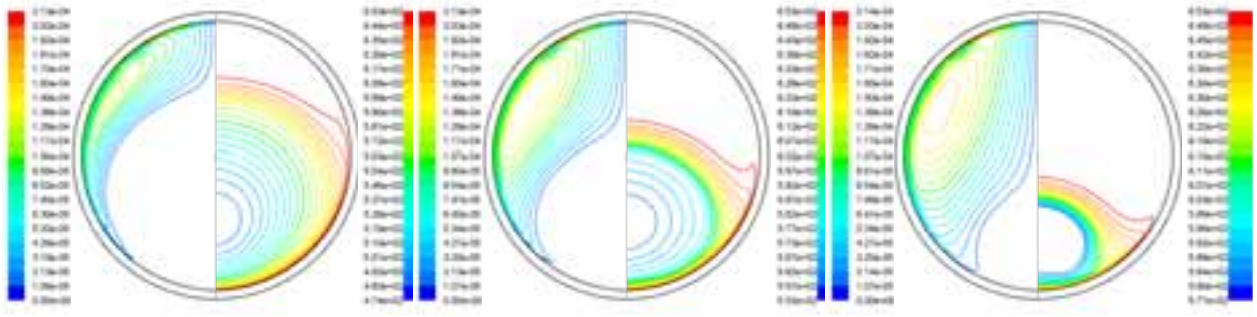

(d) $Ste * Fo = 1.81x10^{-1}$ (e) $Ste * Fo = 2.68x10^{-1}$ (f) $Ste * Fo = 3.48x10^{-1}$

Figure 3: Computed streamlines and temperature contours for case S_2 at different time instants.

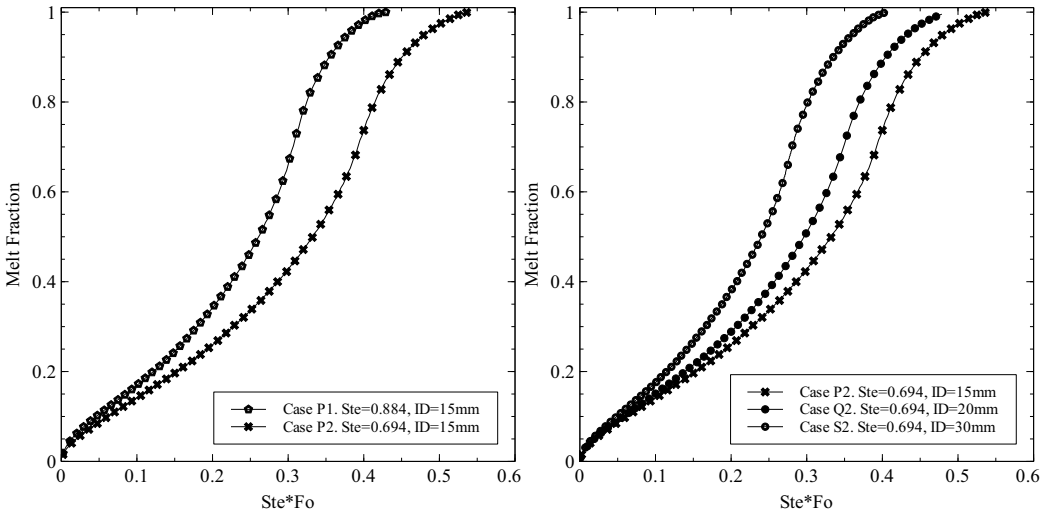

(a) Cases P_1 and P_2 (b) Cases P_2, Q_2 and S_2.

Figure 4: Predicted melt fraction rate for different cases.

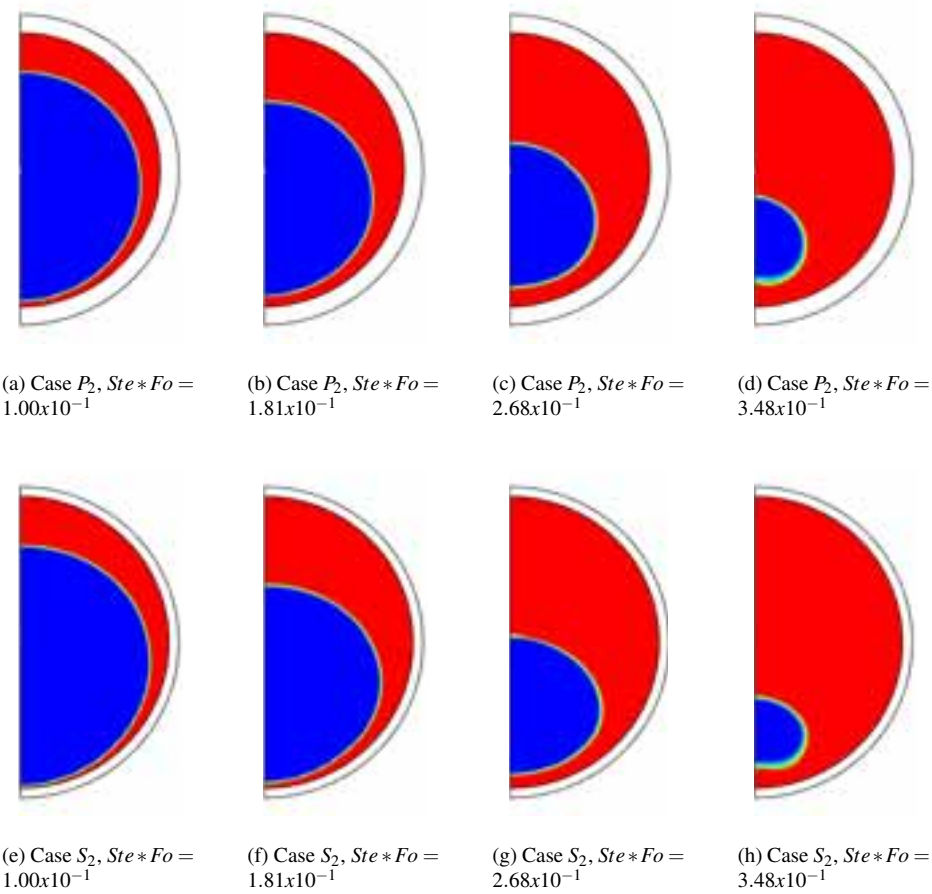

(a) Case P_2, $Ste*Fo = 1.00x10^{-1}$ (b) Case P_2, $Ste*Fo = 1.81x10^{-1}$ (c) Case P_2, $Ste*Fo = 2.68x10^{-1}$ (d) Case P_2, $Ste*Fo = 3.48x10^{-1}$

(e) Case S_2, $Ste*Fo = 1.00x10^{-1}$ (f) Case S_2, $Ste*Fo = 1.81x10^{-1}$ (g) Case S_2, $Ste*Fo = 2.68x10^{-1}$ (h) Case S_2, $Ste*Fo = 3.48x10^{-1}$

Figure 5: Solid/Liquid interface evolution for cases P_2 and S_2.

5. Concluding Remarks

Diffusion-natural convective controlled heat transfer during unconstrained melting process within an encapsulate spherical capsule filled with sodium nitrate was numerically investigated. The following conclusions are drawn:

- Based on the flow field and the solid liquid interface evolution for a fixed Stefan number (Ste=0.694), it can be inferred that the Rayleigh number, when changed from $9.17\text{x}10^6$ to $7.33\text{x}10^7$ increases the melting rates of sodium nitrate. Therefore, it can be inferred that for a fixed Stefan number (Ste=0.694) the melting time increase with decrease in Rayleigh numbers.
- It was found that a recirculating vortex was formed between the top region of the solid phase and the inner wall of the capsule that causes a more intensive melting process in the upper part of the solid phase.

6. Acknowledgments

The project this paper is based on was funded by:

- The State of Florida through the Florida Energy System Consortium (FESC) funds.
- E.ON as part of the E.ON International Research Initiative. Responsibility for the content of this publication lies with the author.

References

[1] Assis, E., Katsman, L., Ziskind, G., Letan, R., 2007. Numerical and experimental study of melting in a spherical shell. International journal of heat and mass transfer 50, 1790–1804.

[2] Bahrami, P., Wang, T., 1987. Analysis of gravity and conduction-driven melting in a sphere. Journal of Heat Transfer (Transactions of the ASME (American Society of Mechanical Engineers), Series C);(United States) 109.

[3] Bareiss, M., Beer, H., 1984. An analytical solution of the heat transfer process during melting of an unfixed solid phase change material inside a horizontal tube. International journal of heat and mass transfer 27, 739–746.

[4] Brent, A., Voller, V., Reid, K., 1988. Enthalpy-porosity technique for modeling convection-diffusion phase change: Application to the melting of a pure metal. Numerical Heat Transfer 13, 297–318.

[5] Dewitt, D., Incropera, F., Bergman, T., 1996. Fundamentals of heat and mass transfer. John Wiley & Sons: New York .

[6] Dutil, Y., Rousse, D., Salah, N., Lassue, S., 2010. A review on phase-change materials: Mathematical modeling and simulations. Renewable and Sustainable Energy Reviews .

[7] Eyres, N., Hartree, D., Ingham, J., Jackson, R., Sarjant, R., Wagstaff, J., 1946. The calculation of variable heat flow in solids. Philosophical Transactions of the Royal Society of London. Series A, Mathematical and Physical Sciences 240, 1–57.

[8] Fomin, S., Saitoh, T., 1999. Melting of unfixed material in spherical capsule with non-isothermal wall. International journal of heat and mass transfer 42, 4197–4205.

[9] Grimado, P., Boley, B., 1970. A numerical solution for the symmetric melting of spheres. International Journal for Numerical Methods in Engineering 2, 175–188.

[10] Khodadadi, J., Zhang, Y., 2001. Effects of buoyancy-driven convection on melting within spherical containers. International journal of heat and mass transfer 44, 1605–1618.

[11] Medrano, M., Gil, A., Martorell, I., Potau, X., Cabeza, L., 2010. State of the art on high-temperature thermal energy storage for power generation. part 2–case studies. Renewable and Sustainable Energy Reviews 14, 56–72.

[12] Moore, F., Bayazitoglu, Y., 1982. Melting within a spherical enclosure. Journal of Heat Transfer 104, 19.

[13] Nicholas, D., Bayazitoğlu, Y., 1980. Heat transfer and melting front within a horizontal cylinder. Journal of Solar Energy Engineering 102, 229.

[14] Nunes, V., Lourenço, M., Santos, F., de Castro, C., 2006. Viscosity of molten sodium nitrate. International journal of thermophysics 27, 1638–1649.

[15] Price, P., Slack, M., 1954. The effect of latent heat on numerical solutions of the heat flow equation. British Journal of Applied Physics 5, 285.

[16] Roy, S., Sengupta, S., 1987. The melting process within spherical enclosures. Journal of heat transfer 109, 460–462.

[17] Roy, S., Sengupta, S., 1990. Gravity-assisted melting in a spherical enclosure: effects of natural convection. International Journal of Heat and Mass Transfer 33, 1135–1147.

[18] Saitoh, T., Kato, K., 1993. Experiment on melting in heat storage capsule with close contact and natural convection. Experimental thermal and fluid science 6, 273–281.

[19] Tan, F., Hosseinizadeh, S., Khodadadi, J., Fan, L., 2009. Experimental and computational study of constrained melting of phase change materials (pcm) inside a spherical capsule. International Journal of Heat and Mass Transfer 52, 3464–3472.

[20] Voller, V., Prakash, C., 1987. A fixed grid numerical modelling methodology for convection-diffusion mushy region phase-change problems. International Journal of Heat and Mass Transfer 30, 1709–1719.

[21] Voller, V., Swenson, J., Kim, W., Paola, C., 2006. An enthalpy method for moving boundary problems on the earth's surface. International Journal of Numerical Methods for Heat & Fluid Flow 16, 641–654.

[22] Wang, S., Faghri, A., Bergman, T., 2010. A comprehensive numerical model for melting with natural convection. International Journal of Heat and Mass Transfer 53, 1986–2000.

[23] White, L., Davis, H., 1967. Thermal conductivity of molten alkali nitrates. The Journal of Chemical Physics 47, 5433.

[24] Zhang, Y., Khodadadi, J., Shen, F., 1999. Pseudosteady-state natural convection inside spherical containers partially filled with a porous medium. International journal of heat and mass transfer 42, 2327–2336.